Journal of Inorganic and Organometallic Polymers and Materials (2023) 33:1409–1414
https://doi.org/10.1007/s10904-023-02589-w

RESEARCH

Cd(II)-Based Complex Constructed from 1,3,5-Tris(Carboxymethoxy) Benzene Acid Ligand for Detection of Nitroaromatic Compounds

Ying-Jun Chen[1] · Xue-Jing Zhai[1] · Wei-Li Wu[1] · Bo Li[1] · Li-Ya Wang[1]

Received: 23 December 2022 / Accepted: 20 February 2023 / Published online: 19 March 2023

Abstract
In this study, one Cd(II)-based complex, $[Cd_3(L)_2(bpy)_2]_n$ (**1**) (L^{3-} = 1,3,5-tris(carboxymethoxy)benzene acid), has been hydrothermally synthesized, which displayed three-dimensional (3D) supramolecular framework. The result of fluorescence quenching experiments revealed that complex **1** showed good quenching effect on nitroaromatic compounds, such as p-nitroaniline (4-NA), o-nitroaniline (2-NA), p-nitrophenol (4-NP), and the quenching effect of 4-NA were particularly significant. According to the density functional theory, the remarkable quenching efficiency of 4-NA was caused by an effective electron transport. As a fluorescent probe, Complex **1** can be used to find nitroaromatic chemicals.

Keywords Cd(II)-based complex · Detection · Nitroaromatic compounds

1 Introduction

Nitroaromatic compounds (NACs) are important agents for environment pollution [1–3], which are formed by incomplete oxidation of organic matter and coexist in various industrial and agricultural discharges [3, 4]. The strong biological toxicity, high stability and poor biodegradability have greatly damaged the environment [5]. Nitrobenzene is the simplest and basic ingredient in the explosive family, and its killing effect cannot be ignored. Therefore, the development of a fast and effective method for detecting nitroaromatic compounds is a hot research topic [6, 7]. Numerous d^{10} metal ions, particularly Zn^{2+} and Cd^{2+} ions, have strong complexation affinities for N/O- donor atoms as well as favourable photoactive characteristics [8, 9]. Because of their fascinating framework architectures, metal–organic frameworks (MOFs) have been developed quickly in research on gas storage/separation, optics, dye capture and catalysis over the last few decades [10–16]. And the literature shows that MOF composed of and electron-rich ligands is more sensitive to nitro aromatic explosives [17–20]. The pore structure of MOF can be effectively adjusted by introducing various functions, such as $-NH_2$, $-CONH_2$, binaphthol and pyridyl, to improve the detection performance of analytes.

Based on these considerations, the tripodal 1,3,5-tris(carboxymethoxy)benzene acid (H_3L) (Scheme 1) and 2,2'-bipyridine are selected as ligands. According to pH, H_3L can be fully or incompletely deprotonated making possible the creation of coordination polymers with a variety of topologies. In addition, the flexibility of $-OCH_2-$ spacers in the carboxylic acid ligand facilitates diverse coordination modes with metal centers. The constructed $[Cd_3(L)_2(bpy)_2]_n$ (**1**) displayed two-dimensional layer structure and further linked into three-dimensional (3D) supramolecular framework through π···π stacking interactions. As expected, complex **1** effectively detects electron-deficient nitro aromatic explosives and is highly sensitive to p-nitroaniline (4-NA). The result of theoretical calculation revealed that the efficient electron transfer led to high quenching efficiency of 4-NA. Thus, complex **1** effectively detects electron-deficient nitro aromatic explosives and is highly sensitive towards p-nitroaniline (4-NA), and the result of theoretical calculations revealed the efficient electron transfer mechanism and quenching efficiency of 4-NA.

✉ Bo Li
libony0107@nynu.edu.cn

✉ Li-Ya Wang
wly@nynu.edu.cn

[1] College of Chemistry and Pharmaceutical Engineering, Nanyang Normal University, 473061 Nanyang, People's Republic of China

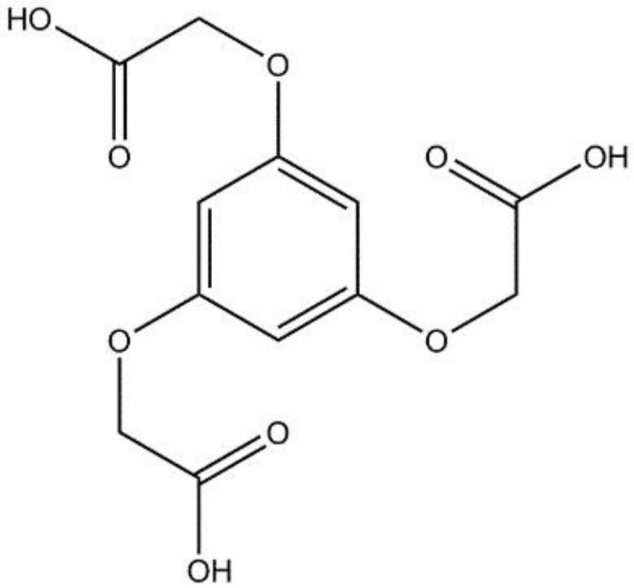

Scheme 1 The diagram of 1, 3, 5-tris(carboxymethoxy) benzene ligand

2 Experimental

2.1 Materials and Instrumentation

The H_3L ligand and other chemicals were bought through commercial means without further purification. The IR spectra of KBr pellets were captured on a Nicolet Avatar-360 spectrometer. The elemental analyses were carried out on a Flash 2000 elemental analyzer. TGA was tested in a nitrogen atmosphere using the SDT 2960 thermal analyzer. By using the UV-2600 UV/VIS spectrophotometer and the CARY Eclipse fluorescence spectrophotometer, solid UV and fluorescence measurements were taken, respectively. Density functional theory (DFT) is used to do the theoretical computation with a B3LYP/6–31 + G* accuracy level using the Gaussian 09 W software package.

2.2 Synthesis of $[Cd_3(L)_2(bpy)_2]_n$(1)

H_3L (0.025 mmol, 7.5 mg), $Cd(CH_3COO)_2{\cdot}2H_2O$ (0.05 mmol, 13.33 mg), and 2,2'-bipy (0.05 mmol, 7.80 mg) were added into N,N-dimethylacetamide (3 mL) and H_2O (2 mL). The mixture was placed in a Teflon-lined autoclave, heated at 120 ºC for 72 h, before cooling to room temperature. Colorless block crystals of **1** were obtained. Anal. Calcd for $C_{44}H_{34}Cd_3N_4O_{18}$: C 42.48, H 2.75, and N 4.50; Found: C 42.51, H 2.72, and N 4.53. IR/cm^{-1} (KBr): 1597(s), 1421(m), 1323(m), 1152(s), 1063(m), 836(w), 764(s), 716(m), 647(s), and 587(s) of (s).

Table 1 Crystallographic data for complex **1**

Complex	1
Formula	$C_{44}H_{34}Cd_3N_4O_{18}$
CCDC	2,227,057
Formula weight	1243.95
Crystal system	Monoclinic
Space group	*C2/c*
a /Å	27.7108(8)
b /Å	10.2359(3)
c /Å	15.6463(5)
α /°	90
β /°	100.747(3)
γ /°	90
Volume /$Å^3$	4360.2(2)
Z	4
Absorption coefficient (mm^{-1})	1.535
F(000)	2456
Refl. collected	9101
Unique	3839
R (int)	0.0197
Data / restraints / parameters	3839 / 18 / 313
GOF on F^2	1.031
R indices [$I > 2\sigma(I)$]	$R_1 = 0.0356$, $wR_2 = 0.1206$
R indices (all data)	$R_1 = 0.0400$, $wR_2 = 0.1293$
Largest diff. peak and hole (e $Å^{-3}$)	1.243 and − 0.691

2.3 Photoluminescence Experiment

In the fluorescence quenching experiment, powder sample (3 mg) of **1** was ultrasonically dispersed in deionized water (3 mL) for 30 min. At the excitation of 285 nm, the newly prepared nitro explosive solution (100 ppm) was added incrementally, and then measured the fluorescence.

2.4 X-ray Crystallography

Diffraction data of complex **1** were collected on an Oxford Diffraction SuperNova diffractometer outfitted with graphite-monochromated Mo-Kα radiation (λ = 0.71073 Å) [21]. CrysAlisPro was used to data collection and processing. SADABS program was utilized for an empirical absorption correction [22]. The structure was solved by direct methods and refined using full matrix least squares on F^2 using the SHELXTL software [23]. Table 1 displays crystallographic data of complex **1** and Table S1 showed a selection of bond lengths and angles.

3 Results and Discussion

3.1 Description of Crystal Structure of 1

The asymmetric unit of complex **1** contains two Cd(II) atoms, a completely deprotonated acid and a 2,2'-bipy (Fig. 1a).

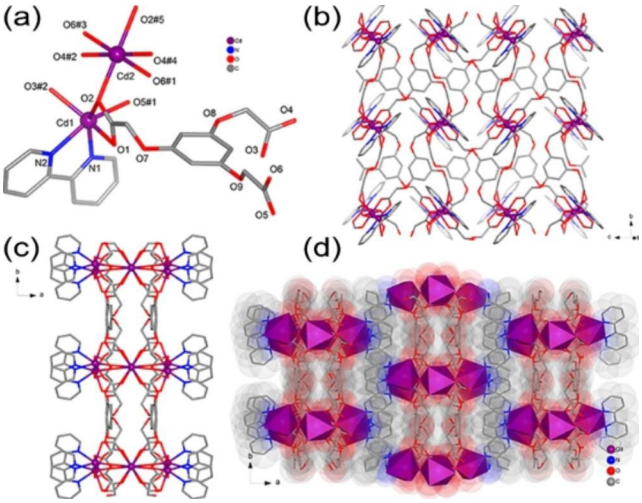

Fig. 1 (a) Coordination environment of Cd(II) in complex **1**. (b, c) Two-dimensional layers of complex **1**. (d) 3D network linked by π···π stacking interactions. Symmetry codes: # 1: x, - y + 1, z – 1/2; # 2: x, y -1, z; # 3: - x, y – 1, - z + 1/2; # 4: – x, – y + 1, - z; # 5: - x, - y, - z

Both metal ions show an octahedral geometry. Cd1 is chelated by 2,2'-bipy ligand and four O atoms from three symmetry related L^{3-} ligands in a highly distorted octahedron, while Cd2 located on a center of symmetry is surrounded by six O atoms from symmetry related L^{3-} ligands. The fully deprotonated acid ligand displays two of μ_2-η^1:η^1 and one of μ_2-η^1:η^2 coordination modes. Cd1-N bond distances are comparable, of 2.338(4) and 2.347(4) Å, while the Cd-O bonds lengths range from 2.189(3) to 2.452(3) Å. The N/O-Cd1-N/O angles range from 53.77(10) to 154.75(13)°, while O-Cd2-O values are close to an almost regular octahedron. As illustrated in Fig. 1b and c, the crystal packing shows a two-dimensional layered structure comprising trinuclear Cd1-Cd2-Cd1' cluster connected by carboxylic ligands, where the Cd1-Cd2 distance is 3.819(6) Å [24].

3.2 Characterization and Fluorescence Stability Study of 1

The experimental results of PXRD diffraction show that the main powder diffraction peak positions of complex **1** are basically consistent with that of theoretical simulation, suggesting the high phase purity of complex **1** (Fig. 2a).

Owing the strong fluorescence of d^{10}-based coordination polymers, the solid-state fluorescence of carboxylic acid ligand and compound **1** were measured (Fig. S1). Strong emission of carboxylic acid ligand can be seen at 302 nm (λ_{ex} = 260 nm), while strong emission of complex **1** can be observed at 438 nm (λ_{ex} = 285 nm). A clear red-shift of 136 nm can be observed comparison to free carboxylic acid ligand, which may result from the electron transfer triggered by the binding of ligand to metal ion [25]. To investigate the fluorescence stability of complex **1**, the sample was immersed in water with different pH value (pH = 3–12). From Fig. 2b, the fluorescence intensity of complex **1** only have small change at different pH value, suggested that complex **1** has good chemical and fluorescence stability.

4 Photoluminescence

To explore the quenching efficiency of **1** to NACs, the fluorescence quenching experiments were carried out by increasing the amount of explosive in the water dispersion of complex **1**. Five nitroaromatic compounds (Scheme S2), p-nitroaniline (4-NA), o-nitroaniline (2-NA), p-nitrophenol (4-NP), 3-nitrophenol (3-NP) and m-dinitrobenzen (1,3-DNB), were chosen to investigate the quenching efficiency of **1**. For each luminescent sensing study, the grounded sample of **1** (3 mg) was added into a 3 mL aqueous solution containing nitroaromatic compound. The findings revealed that complex **1** had diverse fluorescence quenching effects on five distinct nitrobenzene compounds (Fig. 3a). The quenching efficiency of 4-NA (100 ppm) is up to 95.37%,

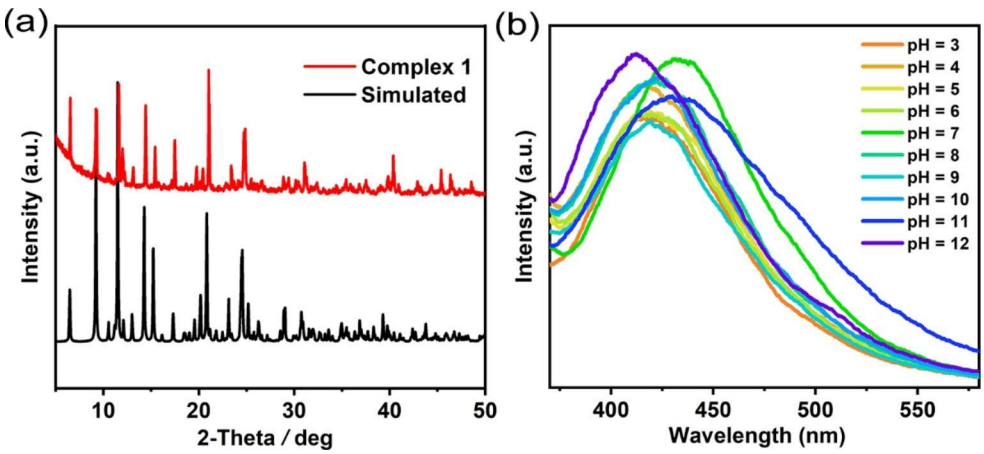

Fig. 2 (a) The PXRD of complex **1**. (b) Fluorescence response of complex **1** at different pH

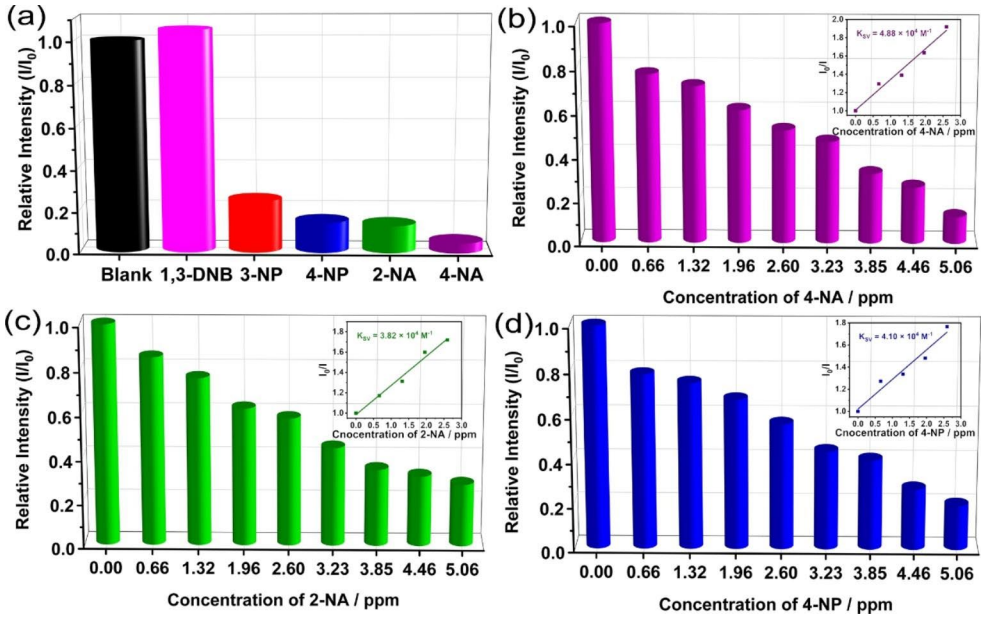

Fig. 3 (a) Fluorescence intensities of complex **1** dispersed in water solution with various NACs (100 ppm). (b-d) Relative emission peak intensity of complex **1** in the presence of different concentrations of NACs. Inset: Stern – Volmer plot of complex **1**

much more than other NACs. The quenching efficiency of 2-NA and 4-NP is 87.06% and 85.64%, respectively.

To test the influence of complex **1** on the detection of 4-NA, 2-NA, and 4-NP in detailed, the quantitative analysis experiments were performed. The prepared NACs solution (20 µL, 100 ppm) was mixed with powder sample **1** (3 mg) ultrasonically dispersed in distilled water (3 mL). As depicted in Fig. 3b and d, the fluorescence intensity declines with incremental addition of 4-NA, 2-NA and 4-NP solution. The equation $I_0/I = K_{sv}[A] + 1$ was utilized to calculate Sterne-Volmer (SV) data of complex **1** for 4-NA, 2-NA and 4-NP solution, where I_0 and I are the luminous intensities before to and following analyte incorporation, respectively. [A] is the analyte concentration, and K_{sv} is the Sterne-Volmer constant (M^{-1}) [26]. A strong linear relationship between the concentration of 4-NA, 2-NA, and 4-NP and the luminous intensity may be seen in the low concentration range. The SV plot demonstrates that the Ksv values of complex **1** for 4-NA, 2-NA and 4-NP are 4.88×10^4 M^{-1}, 3.82×10^4 M^{-1} and 4.10×10^4 M^{-1}, respectively. The relative limits of detection (LODs) for 4-NA, 2-NA, and 4-NP are 5.78×10^{-6} M, 7.69×10^{-6} M, and 7.17×10^{-6} M, respectively, based on the 3δ/Ksv ratio (where δ is the standard deviation of three times luminous intensity in the blank solution). These results indicated that complex **1** has high sensitivity to nitroaromatic compounds (Table S2).

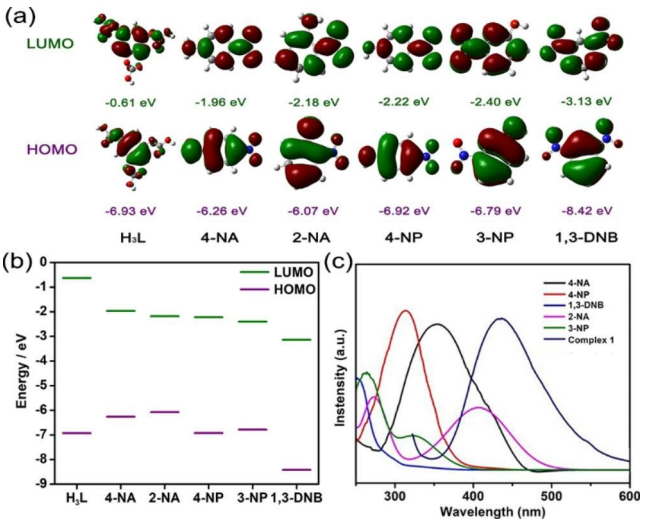

Fig. 4 (a) HOMO and LUMO energy levels of H_3L ligand and the selected NACs calculated by density functional theory (DFT). (b) HOMO and LUMO energies of the H_3L ligand and NACs. (c) Spectral overlaps between the absorption spectra of the NACs and the emission spectra of complex **1**

5 Mechanisms for the Fluorescence Quenching

In order to better understand high sensitivity of complex **1** to NACs, the fluorescence quenching mechanism were explored by theoretical calculation and the UV absorption spectra. The capacity of nitro compounds to absorb electrons allows electrons to be transported from the electron-rich skeleton to NACs. The highest occupied molecular orbital (HOMO) and lowest unoccupied molecular orbital (LUMO) energy levels of ligand and NACs were verified by DFT (Fig. 4a). The LUMO energy of H_3L ligand

is -0.6133 eV, which is higher than that of NACs explosive. Different degrees of fluorescence quenching may arise from the excited electrons in the high LUMO of H_3L being transported to the low LUMO of NACs. The calculated LUMO energy values of NACs are in the order: 4-NA < 2-NA < 4-NP < 3-NP < 1,3-DNB (Fig. 4b), which are consistent with the experimental quenching efficiency. According to the computed outcomes, the 4-NA's excellent quenching efficiency may be attributed to an effective electron transfer.

In order to further confirm this fluorescence quenching mechanism, the UV-Vis absorption spectra of NACs were tested. The efficient overlap between the NACs' absorption band and the MOFs' emission band, as reported in the literature [2, 3], is advantageous for improving the resonance energy transfer's effectiveness in quenching fluorescence. As depicted in Fig. 4c, NACs, particularly 4-NA, showed a strong overlap with complex **1**'s emission band, which was consistent with the fluorescence quenching experiment and theoretical calculation. Therefore, the mechanism of fluorescence quenching may be a synergistic effect of electron transfer mechanism and resonance energy transfer mechanism between complex **1** and NACs [9, 27].

5.1 Stability Analysis

After the fluorescence quenching experiment, the samples dispersed in the solution were collected separately, and washed three times with methanol and distilled water, then placed at room temperature until the water in the sample was completely evaporated to study the PXRD. As shown in Fig. S2, complex **1** still maintained its own MOF structure before and after the fluorescence quenching measurement, indicating the good stability.

6 Conclusion

In summary, a three-dimensional supramolecular network, $[Cd_3(L)_2(bpy)_2]_n$ (**1**), has been designed and synthesized. Complex **1** has not only high selectivity and sensitivity for nitroaromatic explosive, but also good chemical stability. The outcomes showed that complex **1** can be a potential fluorescent probe for nitroaromatic chemical detection. Overall, this work has important reference value and significance for practical application.

Supplementary Information The online version contains supplementary material available at https://doi.org/10.1007/s10904-023-02589-w.

Author Contributions Bo Li, and Li-Ya Wang contributed to the study conception and design. Material preparation, data collection and analysis were performed by Ying-Jun Chen, Xue-Jing Zhai, and Wei-Li Wu. The first draft of the manuscript was written by Ying-Jun Chen and all authors commented on previous versions of the manuscript. All authors read and approved the final manuscript.

Funding We gratefully acknowledge financial support by the National Natural Science Foundation of China (No. U1904199), the Program for Science and Technology Innovation Talents at the University of Henan Province (22HASTIT007), and Nanyang Normal University.

Declarations

Competing Interests The authors have no relevant financial or non-financial interests to disclose.

References

1. T. Zhao, F. Zhang, J. Zhou, X. Zhao, Luminescent Metal-Organic Frameworks for Nitroaromatic Compounds detection. Comment Inorg. Chem. **41**(2), 100–132 (2021)
2. N. Xu, Q. Zhang, G. Zhang, A carbazole-functionalized metal–organic framework for efficient detection of antibiotics, pesticides and nitroaromatic compounds. Dalton Trans. **48**(8), 2683–2691 (2019)
3. X.S. Zeng, H.L. Xu, Y.C. Xu, X.Q. Li, Z.Y. Nie, S.Z. Gao, D.R. Xiao, A series of porous interpenetrating metal–organic frameworks based on fluorescent ligands for nitroaromatic explosive detection. Inorg. Chem. Front. **5**(7), 1622–1632 (2018)
4. S. Pal, P.K. Bharadwaj, A luminescent terbium MOF containing hydroxyl groups exhibits selective sensing of nitroaromatic compounds and fe (III) ions. Cryst. Growth Des. **16**(10), 5852–5858 (2016)
5. Y. Hidalgo-Rosa, K. Mena-Ulecia, M.A. Treto-Suárez, E. Schott, D. Páez-Hernández, X. Zarate, Insights into the selective sensing mechanism of a luminescent cd(II)-based MOF chemosensor toward NACs: roles of the host–guest interactions and PET processes. J. Mater. Sci. **56**(24), 13684–13704 (2021)
6. H.F. Liu, X.H. Qin, F.P. Huang, X.Q. Zhang, H.D. Bian, Threefold interpenetrated metal–organic framework as a multifunctional fluorescent probe for detecting 2, 4, 6-trinitrophenol, levofloxacin, and l-cystine. CrystEngComm. **24**(8), 1622–1629 (2022)
7. Y. Liu, Y. Wang, Y. Zhang, P.G. Karmaker, L. Zhang, F. Huo, X.P. Yang, B. Zhao, Mechanistic insights into the luminescent sensing of nitrophenol compounds by a cationic Zn-based metal-organic framework. Dyes Pigm. **199**, 110099 (2022)
8. D. Tian, Y. Li, R.Y. Chen, Z. Chang, G.Y. Wang, X.H. Bu, A luminescent metal–organic framework demonstrating ideal detection ability for nitroaromatic explosives. J. Mater. Chem. A **2**(5), 1465–1470 (2014)
9. H.F. Chen, X.P. Yang, D.M. Jiang, D. Schipper, R.A. Jones, NIR luminescence for the detection of metal ions and nitro explosives based on a grape-like nine-nuclear nd(III) nanocluster. Inorg. Chem. Front. **6**, 550–555 (2019)
10. X.G. Yang, X.M. Lu, Z.M. Zhai, Y. Zhao, X.Y. Liu, L.F. Ma, S.Q. Zang, Facile synthesis of a micro-scale MOF host–guest with long-lasting phosphorescence and enhanced optoelectronic performance. Chem. Commun. **55**(74), 11099–11102 (2019)
11. X.X. Wu, H.R. Fu, M.L. Han, Z. Zhou, L.F. Ma, Tetraphenylethylene immobilized metal–organic frameworks: highly sensitive fluorescent sensor for the detection of $Cr_2O_7^{2-}$and nitroaromatic explosives. Cryst. Growth Des. **17**(11), 6041–6048 (2017)
12. Y.P. Wu, J.W. Tian, S. Liu, B. Li, J. Zhao, L.F. Ma, D.S. Li, Y.Q. Lan, X.H. Bu, Bi-Microporous Metal-Organic Frameworks with

cubane $[M^4(OH)^4]$(M = Ni, Co) clusters and pore-space partition for electrocatalytic methanol oxidation reaction. Angew Chem. Int. Ed. **58**(35), 12185–12189 (2019)
13. J.H. Qin, W.J. Qin, Z. Xiao, J.K. Yang, H.R. Wang, X.G. Yang, D.S. Li, L.F. Ma, Efficient energy-transfer-induced high photoelectric conversion in a dye-encapsulated ionic pyrene-based metal–organic framework. Inorg. Chem. **60**(24), 18593–18597 (2021)
14. B. Li, H.T. Fan, S.Q. Zang, H.Y. Li, L.Y. Wang, Metal-containing crystalline luminescent thermochromic materials. Coord. Chem. Rev. **377**, 307–329 (2018)
15. G. Tan, R.Q. Jia, X. Zhao, Y.Q. Guo, L.L. Zhang, X.H. Wang, J.G. Wang, X. Feng, B. Li, L.Y. Wang, Fabrication of two Isomorphic and Hyperstable Rare Earth-Based Metal–Organic Frameworks with efficient Ratiometric Probe and Photocatalytic Performances. Inorg. Chem. **61**(30), 11866–11878 (2022)
16. R.Q. Jia, G. Tan, Y.J. Chen, L.Y. Zuo, B. Li, L.Y. Wang, Cu^{II} Ion Doping enhances the Water Stability of luminescent Metal–Organic Framework, realizing the detection of Fe^{3+} and antibiotics in Aqueous Solutions. Front. Chem. **10**, 860232 (2022)
17. C. Zhang, L. Sun, Y. Yan, J. Li, X. Song, Y. Liu, Z.Q. Liang, A luminescent cadmium metal–organic framework for sensing of nitroaromatic explosives. Dalton Trans. **44**(1), 230–236 (2015)
18. P. Karthik, A. Pandikumar, M. Preeyanghaa, M. Kowsalya, B. Neppolian, Amino-functionalized MIL-101 (fe) metal-organic framework as a viable fluorescent probe for nitroaromatic compounds. Mikrochim. Acta **184**(7), 2265–2273 (2017)
19. J. Ye, L. Zhao, R.F. Bogale, Y. Gao, X. Wang, X. Qian, S. Guo, J. Zhao, G. Ning, Highly selective detection of 2, 4, 6-trinitrophenol and Cu^{2+} ions based on a fluorescent cadmium–pamoate metal-organic framework. Chem. Eur. J. **21**(5), 2029–2037 (2015)
20. X.Q. Yao, G.B. Xiao, H. Xie, D.D. Qin, H.C. Ma, J.C. Liu, P.J. Yan, Two triphenylamine-based luminescent metal–organic frameworks as a dual-functional sensor for the detection of nitroaromatic compounds and ofloxacin antibiotic. CrystEngComm. **21**(15), 2559–2570 (2019)
21. J.T. Cosier, A. Glazer, A nitrogen-gas-stream cryostat for general X-ray diffraction studies. J. Appl. Crystallogr. **19**(2), 105–107 (1986)
22. G.M. Sheldrick, *SADABS, Program for Empirical Absorption Correction of area Detector data* (University of Göttingen, Germany, 1996)
23. G.M. Sheldrick, A short history of SHELX. Acta Crystallogr. A **64**(1), 112–122 (2008)
24. X.G. Yang, Z.M. Zhai, X.M. Lu, L.F. Ma, D. Yan, Fast crystallization-deposition of orderly molecule level heterojunction thin films showing tunable up-conversion and ultrahigh photoelectric response. ACS Cent. Sci. **6**(7), 1169–1178 (2020)
25. J.A. Hua, Y. Zhao, Y.S. Kang, Y. Lu, W.Y. Sun, Solvent-dependent zinc(II) coordination polymers with mixed ligands: selective sorption and fluorescence sensing. Dalton Trans. **44**, 11524–11532 (2015)
26. J. Wu, B.H. Li, H.R. Zhong, S.W. Qiu, Y.W. Liang, X.Y. Zhuang, A. Singh, A. Kumar, Fluorescence sensing and photocatalytic properties of a 2D stable and biocompatible zn (II)-based polymer. J. Mol. Struct. **1158**, 264–270 (2018)
27. D.D. Li, J.H. Yu, J.Q. Xu, Synthesis and selective detection towards TNP of two coordination polymers based on ligand generated by in situ acylation reaction. J. Solid State Chem. **293**, 121771–121791 (2021)